Micromagnetic Modeling of Soft Underlayer Magnetization Processes and Fields in Perpendicular Magnetic Recording

Manfred E. Schabes, Byron Lengsfield, and Thomas Schrefl, *Member, IEEE*

***Abstract*—Micromagnetic processes in the soft underlayer (SUL) of a perpendicular magnetic recording medium are studied by dynamic simulation of the Landau–Lifshitz–Langevin equations in order to obtain estimates of the write field as a function of thickness, magnetization, and anisotropy of the SUL. In this way, the SUL thickness requirements are examined from the point of view of supporting a given input magnetic flux. It is shown that insufficient SUL thickness is characterized by large surface charges at the bottom of the SUL, leading to significant external flux leakage. For thicker SULs, the magnetic flux is conducted interior to the SUL and can involve spin-wave excitations with three-dimensional vortices. The wavelength of the spin waves is related to the vortex size and, therefore, to the exchange length of the SUL. The calculations also demonstrate the importance of proper scaling of the solid angle subtended by the write pole as seen by the data layer and SUL when the track density is increased.**

***Index Terms*—Landau–Lifshitz equations, Langevin magnetization dynamics, micromagnetism, perpendicular magnetic recording, soft underlayer.**

I. Introduction

PERPENDICULAR magnetic recording media are being considered for future generations of ultrahigh-density magnetic recording applications. Theoretical predictions of achievable bit densities range from 500 Gb/in^2[1] to 1 Tb/in^2[2] on perpendicular media consisting of a magnetically hard data layer (DL) and a magnetically soft underlayer (SUL). The data layer may be a granular magnetic thin film [3], a multilayer structure [4], or a combination of a granular film with a multilayer structure [5], [6].

Typically, the data layer has a large magnetic anisotropy with easy axis well aligned in the direction perpendicular to the film plane. The soft underlayer has vastly different magnetic properties, in particular, a low magnetic anisotropy and a high magnetization which may be biased to reduce SUL noise [7]. In previous studies, the SUL has generally been much thicker than the data layer.

A perpendicular write head typically consists of a small trailing pole tip P2 and a larger return pole P1. Magnetic transitions are written at the trailing edge of P2 while P1 captures the return flux. The magnetic path between P1 and P2 is bridged by the SUL. In this way, the SUL becomes part of the head structure during the write process. Traditionally, permeability concepts have been applied to describe the conductance of flux in the SUL [8]. However, permeability cannot readily describe micromagnetic processes in the SUL and their nonlinear dependence on SUL moment density, thickness, anisotropy, etc.

Previous micromagnetic models of perpendicular media with soft underlayers have used the method of images, where the contributions of the SUL during writing are modeled by placing magnetostatic image charges in the space occupied by the soft underlayer at mirror planes relative to the top of the SUL [9], [10]. This approach assumes infinite SUL thickness and infinite SUL permeability, although the effects of a finite SUL permeability can be approximated by attenuating the image charge strength by a factor of $(\mu - 1)/(\mu + 1)$[11]. However, it is not possible to determine the minimum SUL thickness and its dependence on the magnetic material parameters of the SUL without further assumptions. Recently, micromagnetic calculations eliminated the need for permeability concepts by solving the micromagnetic differential equations for both the data layer and SUL magnetization [12], [13]. Yet, a finely discretized micromagnetic calculation presents a significant numerical challenge, even for today's supercomputers. For this reason, the discretization size in [12] has been coarse limiting the view of SUL magnetization processes and their causal linkage to magnetic performance. The investigations by Schrefl *et al.* [13] used a fine spatial and temporal finite element discretization for computation of the dynamic hysteresis loops of perpendicular media with a SUL. As shown in [13], the reversal of the SUL can involve complex micromagnetic processes and the excitation of spin waves.

In the present work, we expand on the results of [13] by studying the response of the SUL to the flux of a moving write head as a function of SUL thickness, magnetization, and anisotropy. Section II introduces the micromagnetic model for the data layer and the SUL. Section III presents results for magnetization configurations in the SUL as a function of SUL material parameters and geometrical design parameters including flying height, thickness of the exchange break layer, and size of the write pole. The write field is calculated in the center of the data layer to estimate the maximum admissible dynamic coercivity of the data layer grains.

II. Micromagnetic Model

The perpendicular magnetic recording media modeled in this paper consist of a data layer (DL) with a thickness of 10 nm separated from the soft underlayer (SUL) by an exchange break

Manuscript received November 9, 2001; revised February 22, 2002.

M. E. Schabes and B. Lengsfield are with the IBM Almaden Research Center, San Jose, CA 95120 USA (e-mail: manfred@almaden.ibm.com).

T. Schrefl is with the IBM Almaden Research Center, San Jose, CA 95120 USA and also with the Vienna University of Technology, A-1040 Vienna, Austria.

Publisher Item Identifier S 0018-9464(02)05663-7.

0018-9464/02$17.00 © 2002 IEEE

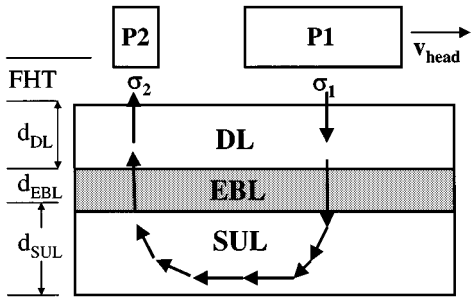

Fig. 1. Model geometry showing magnetic flux flowing through the SUL.

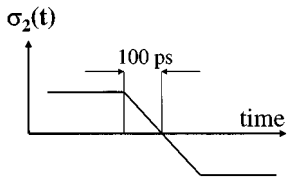

Fig. 2. Temporal profile of the charge density on P2.

layer (EBL) with thickness $d_{\rm EBL}$ where $5 \leq d_{\rm EBL} \leq 20$ nm (Fig. 1). The thickness of the SUL is varied in the range of 20–310 nm. The magnetization of the data layer is 300 emu/cm^3 in all calculations, while SUL magnetizations of 800 and 1350 emu/cm^3 are studied. The exchange in the SUL is 1×10^{-6} erg/cm and the SUL anisotropy field $H_{k,\rm SUL}$ is 10 Oe except in Section III-E, where the effects of larger $H_{k,\rm SUL}$ are investigated. The anisotropy field in the data layer is fixed at 9 kOe and the exchange between DL grains is zero. The DL and SUL are discretized into cubic elements with a uniform size of 10 nm. We used up to 256 by 128 elements per layer (depending on the head size). The largest of the calculations used about 1.04×10^6 elements and a time discretization step of 0.24 ps.

In this work, we focus on the SUL micromagnetics. Thus, we do not consider the details of the head materials but represent the leading pole P1 and the trailing pole P2 by charge sheets with specified magnetic pole densities $\sigma_1(t)$ and $\sigma_2(t)$. The explicit time dependence of σ_1 and σ_2 is given by a trapezoidal function with a linear 100 ps ramp (zero to peak) followed by flat (saturated) plateau, as shown in Fig. 2 and discussed previously in [14]. The charges σ_1 and σ_2 are of opposite sign and are scaled inversely to the cross-sectional areas A_1 and A_2 of P1 and P2 [12]. It is clear that σ_1 and σ_2 represent effective charge densities with $\sigma_1 = \varepsilon_1 M_1$ at P1, and $\sigma_2 = \varepsilon_2 M_2$ at P2. Here, M_1 and M_2 are the magnetizations of P1 and P2; $\varepsilon_i < 1$, $i = 1, 2$, are design specific efficiency factors characterizing the ability of the poles to deliver flux to the tips of P1 and P2. In this paper, we use $M_2 = M_1(A_1/A_2) = 1750$ emu/cm^3 and set $\varepsilon_1 = \varepsilon_2 = 1$. In future work, we will study the changes of ε_1 and ε_2 as a function of SUL properties by also discretizing the pole tips which will then capture all flux paths, including those due to flux leakage along the vertical sides of the pole pieces. In this sense, the present model considers the head as a time-dependent flux source, which is different from the more complicated (and more realistic) case of a time-dependent prescribed magnetomotive force. It is also noted that we do not include eddy currents which can reduce the flux in the SUL when its electrical conductivity is high. Various poles sizes were studied with P2 having a cross section in the range of 140×140 nm^2 to 320×320 nm^2. The cross section of P1 is larger by a factor of 3 to 9 and the separation between P1 and P2 ranged from 260 to 600 nm. The magnetic spacing FHT as shown in Fig. 1 is varied from 10 to 20 nm and includes the mechanical flying height, the overcoats on the media and head, as well as contributions from surface roughness. The linear velocity of the head is fixed at 20 m/s.

In the present model, the total effective field at each point in the data layer and in the SUL can be written as the sum

$$\mathbf{H}_{\rm eff} = \mathbf{H}(t)_{\rm hd} + \mathbf{H}_{\rm an} + \mathbf{H}_x + \mathbf{H}_m + \mathbf{H}_{\rm th} \tag{1}$$

where $H_{\rm eff}$ is the total effective field, $H_{\rm hd}$ is the field from the charge sheets, $H_{\rm an}$ is the anisotropy field, H_x is the exchange field between nearest neighbor elements, H_m is the magnetostatic interaction field due to all the elements of the data layer and soft underlayer, and $H_{\rm th}$ is a thermal fluctuation field computed from the fluctuation-dissipation theorem [15].

Using (1), we solve the magnetodynamic Langevin equations in the Landau–Lifshitz–Gilbert form [16]

$$\frac{d\mathbf{M}}{dt} = -\frac{\gamma}{1+\alpha^2}\mathbf{M} \times \mathbf{H}_{\rm eff} - \frac{\alpha\gamma}{(1+\alpha^2)\,\mathbf{M}_s}\mathbf{M} \times (\mathbf{M} \times \mathbf{H}_{\rm eff}). \tag{2}$$

This system of coupled nonlinear stochastic equations is time integrated in a numerical model which uses the Heun method similar to that of [16]. Equation (2) is solved at a temperature $T = 315$ K on clusters of IBM RISC-6000 workstations and on the IBM SP2 supercomputer at the IBM Watson Research Center.

III. Results

A. Soft Underlayer Magnetization With Saturated Data Layer

In this section, we calculate SUL magnetization configurations as a function of SUL thickness and SUL magnetization. The size of P2 is 240×240 nm^2. The perpendicular component of the head field is in the direction of the data layer magnetization which is kept DC saturated perpendicular to the film plane during the calculations (i.e., we do not attempt to reverse the data layer grains but focus on the case where the self-demagnetization field of the data layer is largest in magnitude and opposite in direction to the head field). This situation is of particular importance since it relates to perpendicular overwrite when the last few grains of the switching field distribution in a bit cell need to be reversed. It is also the field required for closing the major hysteresis loop of a perpendicular film.

The magnetization of the SUL is initially placed in-plane along the radial direction (i.e., the easy anisotropy direction for the SUL). The initial conditions are integrated first without head field for 400 ps, after which the head field is increased along a linear ramp and reaches full strength within 100 ps (Fig. 2). As the head is moving at a velocity of 20 m/s, we continue the integration and capture the magnetization in the SUL after a total elapsed time of 900 ps.

Fig. 3 shows components of the SUL magnetization 500 ps after the start of the head field pulse for $d_{\rm SUL} = 50$ nm. The arrows are scaled proportional to the projection of the magnetiza-

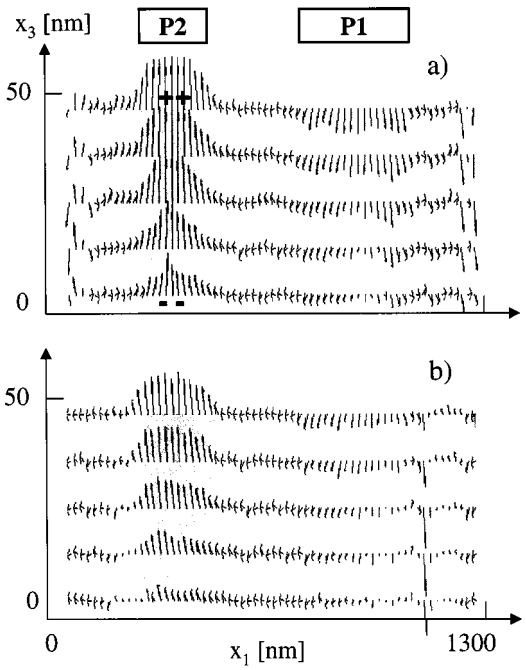

Fig. 3. Soft underlayer magnetization for $d_{\mathrm{SUL}} = 50$ nm. (a) $M_{\mathrm{SUL}} = 800$ emu/cm^3. (b) $M_{\mathrm{SUL}} = 1350$ emu/cm^3.

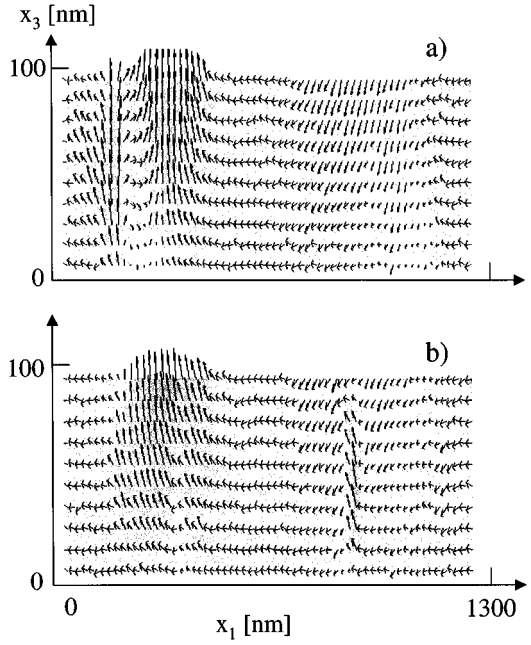

Fig. 4. Soft underlayer magnetization for $d_{\mathrm{SUL}} = 100$ nm. (a) $M_{\mathrm{SUL}} = 800$ emu/cm^3. (b) $M_{\mathrm{SUL}} = 1350$ emu/cm^3.

tion onto the vertical plane in the center of the track. In Figs. 3–5, the magnetization is captured while the head is moving from left to right. In Fig. 3(a), the locations of the write pole P2 and return pole P1 are indicated. In Fig. 3(a) the magnetization is 800 emu/cm^3 and 1350 emu/cm^3 in Fig. 3(b). A combination of small SUL thickness and relatively low SUL magnetization in Fig. 3(a) evidently is not able to carry the magnetic flux input from the head. This leads to a broad region of saturated magnetization directly below P2. The saturated region extends to the bottom of the SUL where a significant amount of magnetic charge is formed as indicated by the plus and minus signs in Fig. 3(a). It is clear that the charges on the top surface increase the write field. However, the charges on the bottom of the SUL are of opposite sign and, therefore, always diminish the write field. Much of the physics and design of the SUL can be understood in terms of maximizing the "good" top surface charges while minimizing the "bad" charges on the bottom of the SUL.

In Fig. 3(b), the magnetization is increased to 1350 emu/cm^3 in an attempt to improve flux flow in the SUL. Now the lateral thickness of the region of high SUL saturation decreases somewhat as a function of increasing depth into the SUL but still pierces the bottom of the SUL generating significant surface charge and exterior flux leakage.

Next, we increase the thickness of the SUL to 100 nm and examine the improvements in flux conductance. The resulting SUL magnetization configurations are shown in Fig. 4. We observe in Fig. 4(a) that a narrowing channel of saturated magnetization reaches the bottom of the SUL for $M_s = 800$ emu/cm^3, indicating that there is still some flux leakage. We also note that as the head is moving to the right, there is a small transient vortex to the left of P2. This vortex pierces the top surface and sends a localized flux spike to the data layer. These transient SUL vortices are observed intermittently at various stages of the write process. These SUL vortices are equivalent to transient parasitic pseudoheads near P2 and P1, which can even lead to irreversible switching of data layer grains depending on the vortex size and properties of the data layer. Vortex fluctuations of this type represent a mechanism for SUL-induced write noise. This is generally different from the read noise that is commonly associated with SUL domains that are detected by the read sensor in addition to the signal from the data layer grains. We expect SUL vortex formation to be influenced by the thickness, anisotropy, and exchange length of the SUL as discussed below. The case of $d_{\mathrm{SUL}} = 100$ nm and $M_{\mathrm{SUL}} = 1350$ emu/cm^3 is shown in Fig. 4(b). In this case, the saturated region below P2 no longer reaches the bottom of the SUL and there is almost no flux leakage.

Further increase in SUL thickness leads to even better flux containment but also to more complicated, time-dependent micromagnetic configurations in the SUL. In Fig. 5, we increase the thickness of the SUL to 300 nm. Most of the flux is contained in the SUL for both 800 and 1350 emu/cm^3. In particular, the SUL with 1350 emu/cm^3 shows pronounced three-dimensional vortices. This can be understood by considering the exchange length $\lambda_{\mathrm{ex}} = (\sqrt{A}/M_s)$, which scales the volume required for formation of magnetostatically driven vortex structures [17]. Inspection of Fig. 5 also reveals the collective spin-wave-like spatial oscillations of the magnetization of the SUL. The wavelength of these oscillations is reduced for the higher magnetic moment density of Fig. 5(b) consistent with the reduction of the exchange length by a factor of about 0.6.

B. Characterization of the Write Field

The total write field H_{write} is defined here as

$$\mathbf{H}_{\mathrm{write}} = \mathbf{H}_w + \mathbf{H}_{\mathrm{DL}} \tag{3}$$

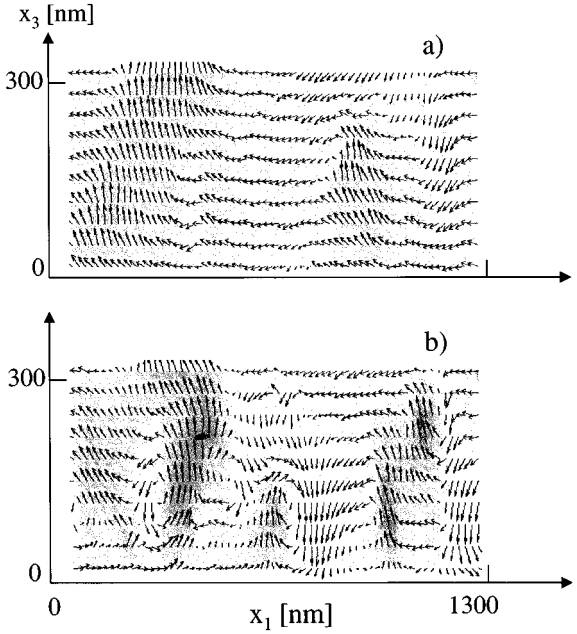

Fig. 5. Soft underlayer magnetization for $d_{\rm SUL} = 310$ nm. (a) $M_{\rm SUL} = 800$ emu/cm^3. (b) $M_{\rm SUL} = 1350$ emu/cm^3.

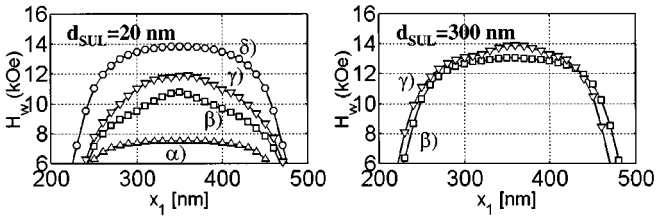

(a) (b)

Fig. 6. Field profiles for (a) $d_{\rm SUL} = 20$ nm and (b) $d_{\rm SUL} = 300$ nm; (α) without SUL contributions, (β) $M_{\rm SUL} = 800$ emu/cm^3, (γ) $M_{\rm SUL} = 1350$ emu/cm^3, (δ) perfect imaging.

with

$$\mathbf{H}_w = \mathbf{H}_{\rm hd} + \mathbf{H}_{\rm SUL}. \tag{4}$$

$H_{\rm DL}$ is the demagnetizing field of the data layer, $H_{\rm hd}$ is the field due to the head poles, and $H_{\rm SUL}$ is the field due to the magnetic polarization charges induced in the soft underlayer. As explained in Section II, $H_{\rm hd}$ is replaced in this paper by the field due to the charge sheets σ_1 and σ_2. In Section III-B–E, we calculate H_w at the center plane of the data layer along the downtrack direction in the center of the track width of P2 while keeping the data layer magnetization fixed.

H_w is plotted in Fig. 6 for $d_{\rm SUL} = 20$ nm and $d_{\rm SUL} = 300$ nm with P2 having a cross section of 240×240 nm^2. In Fig. 6(a), we also compare the micromagnetic calculations with perfect imaging results and with the field profile generated by P2 alone. The case of perfect imaging corresponds to the field solution with $d_{\rm SUL} = \infty$, and SUL permeability $\mu_{\rm SUL} = \infty$, which provides the maximum H_w. The lower limit of the bare head field delineates the case of a thin SUL with low moment density or the case of single-layer perpendicular magnetic recording. Fig. 6(a) shows that at $d_{\rm SUL} = 20$ nm, the maximum of H_w is about 79% and 86% of the perfect imaging field for $M_{\rm SUL} =$ 800 and 1350 emu/cm^3, respectively. H_w is seen to diminish rapidly toward the track edges. If $d_{\rm SUL}$ is increased to 300 nm [Fig. 6(b)], the maximum of H_w for $M_{\rm SUL} = 800$ reaches about 93% of the perfect imaging field, while $M_{\rm SUL} = 1350$ emu/cm^3 nearly matches the perfect imaging field near the center. We also note that the rolloff of the field toward the track edges is less severe for $d_{\rm SUL} = 300$ nm for both for $M_{\rm SUL} = 800$ emu/cm^3 and 1350 emu/cm^3.

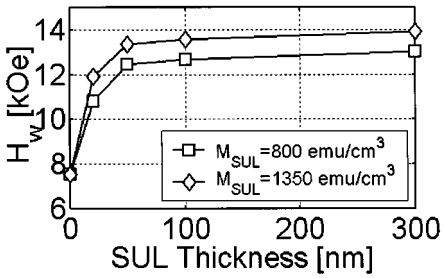

Fig. 7. Maximum magnitude of H_w as a function of SUL thickness for SUL magnetization of 800 and 1350 emu/cm^3.

The dynamic coercivity of the data layer must be chosen in accordance with the magnitude of the write field generated by P2. Fig. 7 shows the maximum field H_w for $M_{\rm SUL}$ of 800 and 1350 emu/cm^3 for $d_{\rm SUL}$ in the range of 20 to 300 nm and P2 having a horizontal cross section of 240×240 nm^2.

A steep initial rise from the bare head field is observed in Fig. 7 for small $d_{\rm SUL}$. The slope of the curves levels off for larger SUL thickness. The soft underlayer with $M_{\rm SUL} = 1350$ emu/cm^3 has a larger initial slope and provides more than 90% of the maximum head field at a modest thickness of about 100 nm. Note that even though the magnetization of the two cases in Fig. 7 differ by 550 emu/cm^3 ($2\pi\Delta M_{\rm SUL} = 3.5$ kOe), H_w increases by only about 1 kOe. In Section III-D, we will show that the field H_w strongly depends on the head size and that larger heads generally require thicker soft underlayers.

C. Dependence of the Write Field on Flying Height, DL Thickness, and EBL Thickness

In this section, we show that the perpendicular write field H_w strongly depends on the flying height due to the fact that the write pole P2 subtends a finite solid angle as seen from the data layer and from the soft underlayer. We also expect a decrease of H_w with increasing thickness of the data layer. In this case, the solid angle subtended by σ_2 decreases at the bottom portion of the data layer grains. This can affect the switching of grains with nonuniform magnetization reversal which is initiated at the top and bottom of high aspect ratio grains [17].

Fig. 8 plots the maximum field H_w under P2 as a function of $d_{\rm SUL}$ for flying heights of 10 and 20 nm and $d_{\rm EBL}$ of 5 and 10 nm. Fig. 8(a) shows that H_w for $M_{\rm SUL} = 800$ emu/cm^3 drops by about 290 Oe, if $d_{\rm EBL}$ is increased from 5 to 10 nm at $d_{\rm SUL} =$ 100 nm. If in addition the flying height is increased to 20 nm, H_w drops by another 590 Oe. A higher $M_{\rm SUL}$ of 1350 emu/cm^3 gives a larger H_w at $d_{\rm SUL} = 100$ nm but also increased absolute sensitivity to spacing. The FHT and EBL losses discussed above increase to 413 and 920 Oe, respectively.

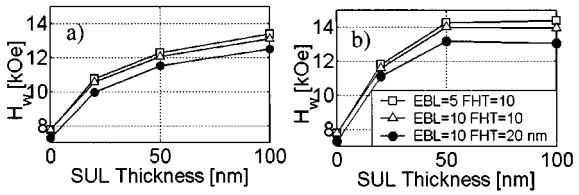

Fig. 8. Maximum magnitude of H_w as a function of $d_{\rm SUL}$ for P2 = 320 × 320 nm^2. (a)$M_{\rm SUL} = 800$ emu/cm^3. (b) $M_{\rm SUL} = 1350$ emu/cm^3.

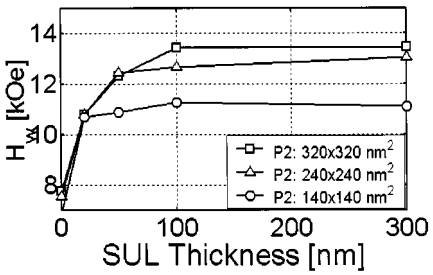

Fig. 9. Maximum field H_w as a function of $d_{\rm SUL}$ for three head sizes at $M_{\rm SUL} = 800$ emu/cm^3.

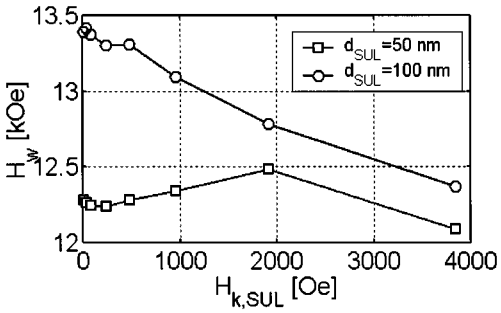

Fig. 10. Maximum H_w as a function of SUL anisotropy field for $d_{\rm SUL} = 50$ nm and $d_{\rm SUL} = 100$ nm.

D. Effect of Head Size

Ultrahigh-density magnetic recording increases the down-track bit density *and* the track density. It is clear from Section III-C that a reduction of track width diminishes the solid angle subtended by P2. Therefore the maximum perpendicular field H_w decreases unless at least one of the parameters FHT, $d_{\rm DL}$, or $d_{\rm EBL}$ is reduced as well (for given SUL).

Fig. 9 compares the maximum H_w for three sizes of P2 for FHT = 10 nm and $d_{\rm EBL} = 5$ nm. The largest P2 in Fig. 9 achieves a maximum H_w of about 13.5 kOe in the data layer. The maximum H_w drops to about 11.1 kOe, if the size of P2 is reduced to 240 × 240 nm^2. These results emphasize the need to scale the spacing parameters (primarily $d_{\rm EBL}$, $d_{\rm DL}$ and FHT) to maintain the desired write field and thermal stability as the track width is reduced.

E. Effect of SUL Anisotropy

SUL domain noise is a major concern for the read process in perpendicular magnetic recording. SUL domain stabilization can be achieved by radial SUL anisotropy fields or by SUL exchange biasing [7]. Fig. 10 plots the maximum field H_w as a function of SUL anisotropy field $H_{k,\rm SUL} = 2K_{\rm SUL}/M_{\rm SUL}$, where $K_{\rm SUL}$ is the anisotropy energy density of the SUL. It is seen in Fig. 10 that H_w is reduced by about 100 Oe at $H_{k,\rm SUL} = 500$ Oe for $d_{\rm SUL} = 100$ nm, while for $d_{\rm SUL} = 50$ nm H_w increases by about 60 Oe at $H_{k,\rm SUL} = 1000$ Oe. In this case H_w has a maximum near $H_{k,\rm SUL} = 2000$ Oe and decreases for larger SUL anisotropy fields.

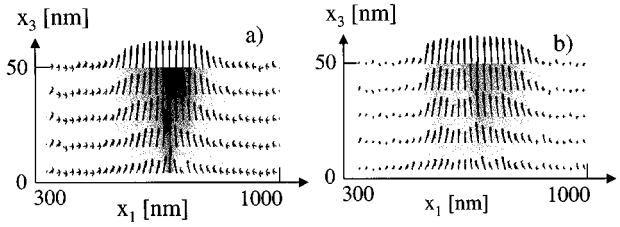

Fig. 11. Magnetization in the SUL below P2 for $d_{\rm SUL} = 50$ nm. (a) $H_{k,\rm SUL} = 10$ Oe. (b) $H_{k,\rm SUL} = 3840$ Oe.

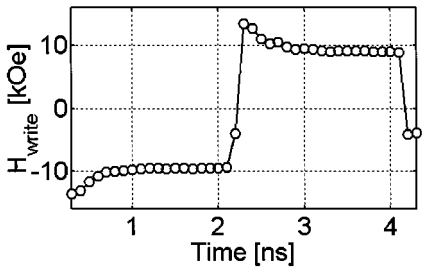

Fig. 12. Time dependence of the total write field during writing of a 40-nm dibit.

Fig. 10 can be understood by considering the competing effects of the magnetostatic charges at the top and bottom of the SUL. For thin SUL the in-plane SUL anisotropy decreases the surface charges at the bottom of the SUL, as shown in Fig. 11. For a range of $H_{k,\rm SUL}$ this effect is larger than the effects due to the reduction of the surface charges at the top of the SUL and a small increase in H_w results. The reduction in charge at the top of the SUL leads to smaller H_w only for rather large $H_{k,\rm SUL}$. However, for a thick SUL there are only small surface charges at the bottom of the SUL and the reduction in the surface charges at the top of the SUL is the dominant effect even at small $H_{k,\rm SUL}$ which leads to a net reduction in field H_w.

F. Write Field During Writing of Transitions

The calculations of Section III-A–F examined the field H_w when the data layer is held saturated. In this section, we investigate the changes in the total write field during the reversal of the DL grains. Fig. 12 shows a temporal profile of the total write field $H_{\rm write}$ during the writing of a dibit of length 40 nm. The size of P2 is 240 × 240 nm^2 and the magnetization of the SUL is 1350 emu/cm^3. The zero of time is chosen to coincide with the start of the plateau of $H_{\rm hd}$ (see Fig. 2). The initial reduction of the write field magnitude in Fig. 12 is due to the self-demagnetizing field $H_{\rm DL}$ which opposes $H_{\rm hd}$ as the data layer magnetization reverses into the direction of $H_{\rm hd}$. This reduction is only about 50% of $8\pi M_{\rm DL}$ due to the small size of the reversed bit and due to the partial saturation of the data layer. Note that $H_{\rm write}$ changes in pace with the rise time of the record current for the thin data layer studied in this paper. We also carried out calculations at different temperatures and found that the initial

response of the SUL can be slower at low temperature. Details of these effects are beyond the scope of the present paper.

IV. Summary

Write field magnitudes in perpendicular magnetic recording with a soft underlayer are strongly affected by the SUL's ability to conduct magnetic flux in its interior. This process can involve spin-wave excitations and micromagnetic vortex structures. Large surface charges at the bottom of the SUL lead to significant flux leakage in the case of insufficient SUL thickness. The calculations also demonstrate the importance of proper scaling of the solid angle subtended by the write pole as seen in the data layer and SUL as the areal bit density is increased.

Acknowledgment

The authors gratefully acknowledge helpful discussions with Dr. D. Newns and Dr. W. Donath of the IBM Watson Research Center, Dr. M. Williams of the IBM Almaden Research Center, as well as with Prof. H. N. Bertram, Dr. H. Zhou, and K. Gao of the University of California, San Diego.

References

[1] H. N. Bertram and M. Williams, "SNR and density limit estimates: A comparison of longitudinal and perpendicular recording," *IEEE Trans. Magn.*, vol. 36, pp. 4–9, Jan. 2000.

[2] R. Wood, "The feasibility of magnetic recording at 1 Terabit per square inch," *IEEE Trans. Magn.*, vol. 36, pp. 36–42, Jan. 2000.

[3] Y. Ikeda, Y. Sonobe, G. Zeltzer, B. K. Yen, K. Takano, E. Do, E. E. Fullerton, and P. Rice, "Medium noise and grain size analysis of CoCrPt/Ti perpendicular media with NiAl seed layer," *IEEE Trans. Magn.*, vol. 37, pp. 1583–1585, July 2001.

[4] W. Peng, R. H. Victora, and J. H. Judy, "Co/Pd and Co/Pt multilayers with indium tin oxide seed layers and NiFe soft underlayers for perpendicular magnetic recording media," *IEEE Trans. Magn.*, vol. 37, pp. 1577–1579, July 2001.

[5] Y. Sonobe, D. Weller, Y. Ikeda, M. Schabes, K. Takano, G. Zeltzer, B. K. Yen, M. E. Best, S. J. Greaves, H. Muraoka, and Y. Nakamura, "Thermal stability and SNR of coupled granular/continuous media," *IEEE Trans. Magn.*, vol. 37, pp. 1667–1670, July 2001.

[6] S. J. Greaves, H. Muraoka, Y. Sonobe, M. Schabes, and Y. Nakamura, "Pinning of written bits in perpendicular recording media," *J. Magn. Magn. Mater.*, vol. 235, pp. 418–423, Oct. 2001.

[7] H. S. Jung and W. D. Doyle, "FeTaN/IrMn exchange coupled multilayer films as soft underlayers for perpendicular media," *IEEE Trans. Magn.*, vol. 37, pp. 2294–2297, July 2001.

[8] R. Wood, J. Monson, and T. Coughlin, "On the thermal decay of magnetization in the presence of demagnetizing fields and a soft magnetic layer," *J. Magn. Magn. Mater.*, vol. 193, pp. 207–12, Mar. 1999.

[9] Q. C. Peng and H. N. Bertram, "Micromagnetic studies of switching speed in longitudinal and perpendicular polycrystalline thin film recording media," *J. Appl. Phys.*, vol. 81, pp. 4384–4386, Apr. 1997.

[10] H. Zhou, H. N. Bertram, and M. E. Schabes, "Micromagnetic analysis of the effect of intergranular exchange on the thermal stability in magnetic recording (III): Perpendicular media," *IEEE Trans. Magn.*, vol. 38, pp. 1422–1428, Mar. 2002.

[11] J. D. Jackson, *Classical Electrodynamics*. New York: Wiley, 1975.

[12] M. Khan and R. H. Victora, "Micromagnetic model of perpendicular recording head with soft underlayer," *IEEE Trans. Magn.*, vol. 37, pp. 1379–1381, July 2001.

[13] T. Schrefl, M. E. Schabes, and B. Lengsfield, "Fast reversal dynamics in perpendicular magnetic recording media with a soft underlayer," presented at the Conf. Magnetism and Magnetic Materials, Seattle, WA, 2001, Paper HA-06.

[14] M. E. Schabes, H. Zhou, and H. N. Bertram, "Effects of head field pulse shape and rise time on subnanosecond magnetization reversal in longitudinal thin film media," *J. Appl. Phys.*, vol. 87, pp. 5666–5668, May 2000.

[15] R. Kubo, "The fluctuation-dissipation theorem," *Rep. Prog. Phys.*, vol. 29, pp. 255–282, 1966.

[16] W. Scholz, T. Schrefl, and J. Fidler, "Micromagnetic simulation of thermally activated switching in fine particles," *J. Magn. Magn. Mater.*, vol. 233, pp. 296–304, Aug. 2001.

[17] M. E. Schabes, "Micromagnetic theory of nonuniform magnetization processes in magnetic recording particles," *J. Magn. Magn. Mater.*, vol. 95, pp. 240–288, 1991.